Banner appropriate to article type will appear here in typeset article

Instability of co-flow in a Hele-Shaw cell with cross-flow varying thickness

John C. Grenfell-Shaw[1]‡‡, Edward M. Hinton[2] and Andrew W. Woods[1]†

[1]BP Institute, University of Cambridge, Madingley Road, Cambridge CB3 0EZ, UK

[2]School of Mathematics and Statistics, The University of Melbourne, Parkville, VIC 3010, Australia

(Received xx; revised xx; accepted xx)

We analyse the stability of the interface between two immiscible fluids both flowing in the horizontal direction in a thin cell with vertically varying gap width. The dispersion relation for the growth rate of each mode is derived. The stability is approximately determined by the sign of a simple expression, which incorporates the density difference between the fluids and the effect of surface tension in the along- and cross-cell directions. The latter arises from the varying channel width: if the non-wetting fluid is in the thinner part of the channel, the interface is unstable as it will preferentially migrate into the thicker part. The density difference may suppress or complement this effect. The system is always stable to sufficiently large wavenumbers owing to the along-flow component of surface tension.

1. Introduction

The parallel co-flow of two fluids occurs in many industrial, biological and environmental processes. It is often important to understand the interfacial instability and develop strategies to control it. Frequently, these flows occur in thin channels whose thickness varies in the cross-flow direction. Examples include: the flow of cement and drilling fluid within a casing pipe of a subsurface well, where the intermingling of cement and mud can produce poorly sealed wells with the attendant risks of leakage; the flow of coatings in the corner region along the line of intersection between two planes, where the displacement of air limits the formation of non-coated zones (Weislogel & Lichter 1996); flows of reactants in microfluidic channels (Sauer 1987; Huang *et al.* 2018); and the displacement of water by CO_2 in permeable channels used for CO_2 sequestration, where intermingling may enhance the efficiency of the sequestration (Woods & Mingotti 2016). For the last example of CO_2 sequestration, the pore-scale dynamics, which are controlled by capillary effects and the interpore geometry are not fully understood but can have a significant effect on macroscale mechanisms such as the flux and the residual trapping of the CO_2, which are key to estimating storage efficiency (Zhao *et al.* 2019; Benham *et al.* 2021). If the initial flow involves the displacement of one fluid by a second along the channel, the displacing fluid will migrate along the wide part of the channel, stretching out the interface; at long times, the interface is approximately directed along the channel, and the flow evolves to the co-flowing geometry of the present problem (c.f. Woods & Mingotti 2016; Mortimer & Woods 2021).

‡‡ Deceased.

† Email address for correspondence: andy@bpi.cam.ac.uk

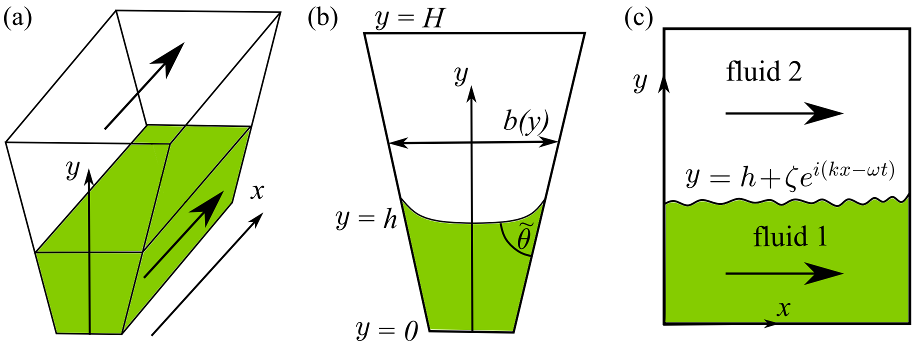

Figure 1: (a) Schematic of the setup. Large arrows indicate the flow direction. (b) Cross-section perpendicular to the x direction. (c) Cross-section in the x direction.

We investigate how the stability of the interface between the two fluids in a thin cell with vertically varying gap width is controlled by cross-layer buoyancy and capillary effects (figure 1). We assume that inertia plays a negligible role in the base flow. It has been shown that when inertia plays a significant role and the two fluids in the Hele-Shaw cell have significantly different viscosities, the shear-controlled Kelvin-Helmholtz instability may occur as has been observed experimentally (Zeybek & Yortsos 1992; Gondret & Rabaud 1997; Rabaud & Moisy 2020). In wider channels, it has been shown that even at zero Reynolds number the vertical shear associated with the no-slip boundaries at the top and bottom can give rise to interfacial instabilities in the co-flow of two fluids of different viscosity (Yih 1967). Similar behaviour can occur in two-layer gravity-driven flow (Loewenherz & Lawrence 1989).

In the present work, we consider a laterally thin cell in which the vertically varying velocity arises from variations in the cell width. The stability is primarily controlled by the density difference between the fluids and surface tension. It is well-established that the along-flow component of surface tension stabilises larger wavenumbers. The combination of surface tension and the cross-cell variation in thickness introduces a new (de)stabilising process for small wavenumbers in the case that the (non-)wetting fluid is in the thinner part of the channel. This effect may complement or suppress the effect of a density difference between the two fluids on the stability of the interface.

The impact of variations in the surface tension associated with variations in the channel width have been explored in detail for the related problem in which an input fluid displaces an ambient fluid in a cell whose width varies in the direction of flow (Homsy 1987; Al-Housseiny *et al.* 2012; Dias & Miranda 2013; Grenfell-Shaw & Woods 2017). These studies have identified that the effect of cross-cell curvature can complement or suppress the classical Saffman-Taylor instability (Saffman & Taylor 1958).

2. Formulation

The flow and the cell geometry is illustrated in figure 1. The cell occupies $0 < y < H$ and has width, $b(y)$, that varies in the vertical direction,

$$b(y) = b_0 + \alpha y, \tag{2.1}$$

where α represents the inclination of the cell walls, which may be positive or negative, and $\alpha > -b_0/H$ so that the cell width is non-negative. Flow is driven in both fluids in the x direction by a background pressure gradient with magnitude G. For relatively slow flows, we can apply the lubrication approximation, which is to say that the leading order velocities are independent of x. Under this assumption, the momentum and continuity equations for the gap-averaged velocity in each fluid take the form (equation 11 of Gondret & Rabaud 1997)

$$\frac{\partial \bar{\boldsymbol{u}}}{\partial t} + \bar{\boldsymbol{u}} \cdot \nabla \bar{\boldsymbol{u}} = -\frac{1}{\rho}\nabla p - \frac{12\mu}{\rho b^2}\bar{\boldsymbol{u}} - g\boldsymbol{e}_y, \qquad \nabla \cdot (b\bar{\boldsymbol{u}}) = 0, \tag{2.2}$$

where, $\nabla = (\partial/\partial x, \partial/\partial y)$, $\boldsymbol{e}_y$ is the unit vector in the y direction and μ and ρ are the fluid viscosity and density, respectively. Also, p is the pressure, g represents gravity, which acts in the negative y direction and $\bar{\boldsymbol{u}} = (\bar{u}, \bar{v})$ is the width-averaged velocity in the x and y directions. The boundary conditions are no-flux at the top and bottom of the channel: $\bar{v} = 0$, whilst at the fluid-fluid interface, $y = y_I$, the velocity in each fluid satisfies the kinematic boundary condition

$$\frac{\partial y_I}{\partial t} + \bar{u}\frac{\partial y_I}{\partial x} = \bar{v}. \tag{2.3}$$

In addition, there is a pressure jump at the interface associated with its curvature, $\kappa = \nabla^2 y_I$, given by

$$\Delta p = \gamma \kappa, \tag{2.4}$$

where γ represents surface tension. The unperturbed steady base flow is given by

$$\bar{u} = U_0(y) = \frac{b(y)^2 G}{12\mu}, \qquad \bar{v} = 0, \qquad p = P_0(x, y) = -\rho g y - Gx + \text{const.} \tag{2.5}$$

The fluids are immiscible and the location of the fluid-fluid interface, $y_I = h$ is a constant for the case of steady flow, which depends on the channel angle, the relative flux in each layer and the viscosity ratio. Although the curvature of the interface in the along-flow direction vanishes since y_I is indepedent of x, there is curvature in the cross-channel direction owing to the contact angle at the wall and the varying channel width (figure 1b). Hence, there is a pressure jump at the interface, which is independent of x, and the constants in P_0 in the base flow are different in the two fluids.

We consider perturbations to the interface and steady base flow of the form

$$y_I = h + \zeta e^{i(kx - \omega t)} \tag{2.6}$$

$$(\bar{u}, \bar{v}) = (U_0(y), 0) + (u(y), v(y))e^{i(kx - \omega t)}, \tag{2.7}$$

$$p = P_0(x, y) + p(y)e^{i(kx - \omega t)}. \tag{2.8}$$

where ζ, $u(y)$, $v(y)$ and $p(y)$ are assumed to be small. We seek to determine the stability of such perturbations. The linearised governing equations in each fluid are

$$-i\omega u + ikU_0 u + vU_0' = \frac{-ikp}{\rho} - \frac{12\mu u}{\rho b^2} \tag{2.9}$$

$$-i\omega v + ikU_0 v = -\frac{p'}{\rho} - \frac{12\mu v}{\rho b^2} \tag{2.10}$$

$$iku b + (vb)' = 0, \tag{2.11}$$

where a prime ($'$) denotes differentiation with respect to y. We eliminate p' to obtain

$$-i\omega u' + ik(U_0 u)' + (vU_0')' - k\omega v + k^2 U_0 v = \frac{12ik\mu v}{\rho b^2} - \frac{12\mu(u/b^2)'}{\rho}. \tag{2.12}$$

Also, continuity yields

$$u = \frac{i(vb)'}{kb} = \frac{i}{k}\left(v' + \frac{v\alpha}{b}\right), \tag{2.13}$$

which can be used to eliminate $u(y)$ from equation (2.12) and obtain a differential equation for $v(y)$,

$$A(y)v'' + B(y)v' + C(y)v = 0, \tag{2.14}$$

where the coefficients are defined below for the dimensionless analogue.

2.1. *Non-dimensionalisation*

To scale the system, we use the tank height, H as the length-scale and the time-scale is $T = \mu_2/(GH)$. The pressure scale is GH. We write

$$(\hat{x}, \hat{y}) = (x, y)/H, \quad \hat{k} = Hk, \quad \hat{w} = Tw, \quad \hat{b}(\hat{y}) = b(y)/H = \hat{b_0} + \alpha\hat{y}, \tag{2.15}$$

with $\hat{b}_0 = b_0/H$, $\hat{h} = h/H$ and $\hat{\zeta} = \zeta/H$. The upper fluid is labelled fluid 2, whilst the lower is labelled fluid 1 (figure 1). Henceforth, all quantities are dimensionless unless stated otherwise and we discard the hat notation. The dimensionless equation in fluid $j = 1, 2$ becomes

$$A^{(j)}(y)v^{(j)}_{yy} + B^{(j)}(y)v^{(j)}_y + C^{(j)}(y)v^{(j)} = 0, \tag{2.16}$$

with coefficients,

$$A^{(j)} = \frac{\omega b(y)^4}{k} - \frac{M_j b(y)^6}{12} + \frac{ib(y)^2 R_j \mathcal{A}}{k} \tag{2.17}$$

$$B^{(j)} = \frac{\omega\alpha b(y)^3}{k} - \frac{M_j \alpha b(y)^5}{12} - \frac{i\alpha b(y) R_j \mathcal{A}}{k} \tag{2.18}$$

$$C^{(j)} = \frac{-\omega\alpha^2 b(y)^2}{k} + \frac{M_j\alpha^2 b(y)^4}{12} - k\omega b(y)^4 + \frac{M_j k^2 b(y)^6}{12} - ikb(y)^2 R_j\mathcal{A} - \frac{3i\alpha^2 R_j \mathcal{A}}{k}, \tag{2.19}$$

where $M_1 = M$, $M_2 = 1$ and $R_1 = R$, $R_2 = M$, and we have introduced the following dimensionless parameters,

$$M = \frac{\mu_2}{\mu_1}, \qquad R = \frac{\rho_2}{\rho_1}, \qquad \mathcal{A} = \frac{12\mu_1\mu_2}{\rho_2 H^3 G}, \tag{2.20}$$

which respectively represent the viscosity ratio, the density ratio and the importance of viscous drag relative to inertia; $\mathcal{A}$ is inversely proportional to a Reynolds number.

2.2. *Boundary conditions*

The perturbed no-flux boundary conditions are

$$v^{(1)}(0) = v^{(2)}(1) = 0. \tag{2.21}$$

The kinematic boundary conditions (2.3) at the fluid-fluid interface become

$$v^{(1)}(h) = i\zeta\left[\frac{b(h)^2 M}{12}k - \omega\right], \qquad v^{(2)}(h) = i\zeta\left[\frac{b(h)^2}{12}k - \omega\right]. \tag{2.22}$$

The dynamic boundary condition at the interface accounts for a jump in pressure associated with surface tension and curvature. This comprises two contributions: the along-channel curvature and the cross-channel curvature. The former is proportional to the second derivative of the interface y_I in the x direction, which furnishes a term proportional to k^2. Treating the cross-channel curvature requires more care. The contact angle, $\tilde{\theta}$, is defined as the angle between fluid 1 and the channel wall (figure 1b). In a cell with inclined walls, the radius of curvature is adjusted from the case of a parallel sided cell and we define an effective contact angle, $\theta = \tilde{\theta} - \phi$, where $\tan\phi = \alpha/2$ (Park & Homsy 1984; Romero & Yost 1996; Grenfell-Shaw & Woods 2017). The discontinuity in the perturbed pressures at the interface is then given by

$$p_2(h) - p_1(h) = C\zeta\left[R - 1 - Bo^{-1}\left(k^2 + \frac{2\alpha\cos\theta}{b(h)^2}\right)\right], \tag{2.23}$$

where we have introduced the following dimensionless groups

$$C = \frac{\rho_1 g}{G}, \qquad Bo = \frac{g\rho_1 H^2}{\gamma}. \tag{2.24}$$

We use the dimensionless analogues of equations (2.9) and (2.13) to obtain the dimensionless pressures in terms of the vertical velocity, v, in each fluid,

$$p_j = \frac{12i\omega}{k^2 R_j M_j \mathcal{A}}\frac{(v^{(j)}b)'}{b} - \frac{i}{k}\frac{b(v^{(j)}b)'}{\mathcal{A}R_j} + \frac{2i\alpha b v^{(j)}}{k\mathcal{A}R_j} - \frac{12}{M_j k^2}\frac{(v^{(j)}b)'}{b^3}. \tag{2.25}$$

We substitute the pressures into the dynamic boundary condition (2.23) to obtain

$$\begin{aligned}
&\alpha v^{(1)}\left(\frac{\omega}{kb} + \frac{Mb}{12} + \frac{iR\mathcal{A}}{kb^3}\right) + \frac{\mathrm{d}v^{(1)}}{\mathrm{d}y}\left(\frac{\omega}{k} - \frac{Mb^2}{12} + \frac{iR\mathcal{A}}{kb^2}\right) \\
&- R\alpha v^{(2)}\left(\frac{\omega}{kb} + \frac{b}{12} + \frac{iM\mathcal{A}}{kb^3}\right) - R\frac{\mathrm{d}v^{(2)}}{\mathrm{d}y}\left(\frac{\omega}{k} - \frac{b^2}{12} + \frac{iM\mathcal{A}}{kb^2}\right) \\
=&\frac{kRM\mathcal{A}i}{12}C\zeta\left[R - 1 - Bo^{-1}\left(k^2 + \frac{2\alpha\cos\theta}{b^2}\right)\right],
\end{aligned} \tag{2.26}$$

where the suppressed argument of $v^{(1)}$, $v^{(2)}$, $\mathrm{d}v^{(1)}/\mathrm{d}y$, $\mathrm{d}v^{(2)}/\mathrm{d}y$ and b is $y = h$.

3. Solution method

The system for $v(y)$ comprises two second order linear ODEs in $0 < y < h$ and $h < y < H$ (2.16) and four boundary conditions: no flux at the top and bottom boundaries (2.21) and the kinematic and dynamic boundary conditions (2.22, 2.26) at the interface. We note that the two equations for the kinematic condition (2.22) can be used to eliminate ζ from the problem. To solve this system, we first simplify the problem by writing $\bar{b}(y) = kb(y)/\alpha$ and obtain the following equation for $v^{(j)}(\bar{b})$,

$$A^{(j)}(y)v^{(j)}_{\bar{b}\bar{b}} + B^{(j)}(y)v^{(j)}_{\bar{b}} + C^{(j)}(y)v^{(j)} = 0, \tag{3.1}$$

with

$$A^{(j)} = a_6^{(j)}\bar{b}^6 + a_4^{(j)}\bar{b}^4 + \bar{b}^2 \tag{3.2}$$

$$B^{(j)} = a_6^{(j)}\bar{b}^5 + a_4^{(j)}\bar{b}^3 - \bar{b} \tag{3.3}$$

$$C^{(j)} = -a_6^{(j)}(\bar{b}^6 + \bar{b}^4) - a_4^{(j)}(\bar{b}^4 + \bar{b}^2) - \bar{b}^2 - 3, \tag{3.4}$$

where we have introduced the following for each fluid,

$$a_6^{(j)} = \frac{-M_j\alpha^4}{12iR_j\mathcal{A}k^3}, \qquad a_4^{(j)} = \frac{\omega\alpha^2}{iR_j\mathcal{A}k^2}. \tag{3.5}$$

The general solution for v in each fluid is given by a linear combination of two independent power series, $\Phi^{(j)}(\bar{b})$ and $\Psi^{(j)}(\bar{b})$, whose coefficients are determined by Frobenius' method (given in Appendix A). The velocities are $(j = 1, 2)$

$$v^{(j)}(y) = c^{(j)}\left(\frac{\Phi^{(j)}(\bar{b}(y))}{\Phi^{(j)}(\bar{b}(j-1))} - \frac{\Psi^{(j)}(\bar{b}(y))}{\Psi^{(j)}(\bar{b}(j-1))}\right), \tag{3.6}$$

where $c^{(j)}$ are constants and we have used the no-flux boundary conditions at the base and the top $(y = j - 1)$. The dynamic boundary condition may be written as (at $y = h$),

$$\frac{(v^{(1)}\bar{b})_{\bar{b}}}{\bar{b}^3} + a_4^{(1)}\frac{(v^{(1)}\bar{b})_{\bar{b}}}{\bar{b}} + a_6^{(1)}\left(\frac{v^{(1)}}{\bar{b}}\right)_{\bar{b}}\bar{b}^3 \tag{3.7}$$

$$- M\left[\frac{(v^{(2)}\bar{b})_{\bar{b}}}{\bar{b}^3} + a_4^{(2)}\frac{(v^{(2)}\bar{b})_{\bar{b}}}{\bar{b}} + a_6^{(2)}\left(\frac{v^{(2)}}{\bar{b}}\right)_{\bar{b}}\bar{b}^3\right] \tag{3.8}$$

$$= \frac{iM\alpha^2 v^{(1)}}{12k\omega}C\left[R - 1 - Bo^{-1}\left(k^2 + \frac{2\alpha\cos\theta}{b^2}\right)\right]\left(\frac{a_6^{(1)}}{a_4^{(1)}}\bar{b}^2 + 1\right)^{-1}. \tag{3.9}$$

The kinematic boundary condition may be written as

$$v^{(1)}\left(\frac{a_6^{(2)}}{a_4^{(2)}}\bar{b}^2 + 1\right) = v^{(2)}\left(\frac{a_6^{(1)}}{a_4^{(1)}}\bar{b}^2 + 1\right). \tag{3.10}$$

Combining the velocities with these two boundary conditions furnishes the following dispersion relation

$$D^{(1)}E^{(1)} - ME^{(2)}D^{(2)} - S = 0, \tag{3.11}$$

where

$$E^{(j)} = \frac{t_j}{\bar{b}^2} + \frac{1}{\bar{b}^3} + a_4^{(j)}\left(t_j + \frac{1}{\bar{b}}\right) + a_6^{(j)}\left(t_j\bar{b}^2 - \bar{b}\right), \tag{3.12}$$

$$D^{(j)} = \frac{a_6^{(j)}}{a_4^{(j)}}\bar{b}^2 + 1, \tag{3.13}$$

$$S = \frac{iM\alpha^2}{12k\omega}C\left[R - 1 - Bo^{-1}(k^2 + 2\alpha\cos\theta/b(h)^2)\right], \tag{3.14}$$

$$t_1 = \frac{\Phi_{\bar{b}}^{(1)}(\bar{b}(h))/\Phi^{(1)}(\bar{b}(0)) - \Psi_{\bar{b}}^{(1)}(\bar{b}(h))/\Psi^{(1)}(\bar{b}(0))}{\Phi^{(1)}(\bar{b}(h))/\Phi^{(1)}(\bar{b}(0)) - \Psi^{(1)}(\bar{b}(h))/\Psi^{(1)}(\bar{b}(0))}, \tag{3.15}$$

$$t_2 = \frac{\Phi_{\bar{b}}^{(2)}(\bar{b}(h))/\Phi^{(2)}(\bar{b}(1)) - \Psi_{\bar{b}}^{(2)}(\bar{b}(h))/\Psi^{(2)}(\bar{b}(1))}{\Phi^{(2)}(\bar{b}(h))/\Phi^{(2)}(\bar{b}(1)) - \Psi^{(2)}(\bar{b}(h))/\Psi^{(2)}(\bar{b}(1))}, \tag{3.16}$$

where i is the imaginary unit. For any value of k and the dimensionless parameters, we may obtain a solution for the growth rate, ω that satisfies equation (3.11) (e.g. figure 2a).

4. Analysis

The terms in the square brackets in S (equation 3.14) correspond to the pressure jump at the interface and we define

$$J = R - 1 - Bo^{-1}\left[k^2 + 2\alpha\cos\theta/b(h)^2\right]. \tag{4.1}$$

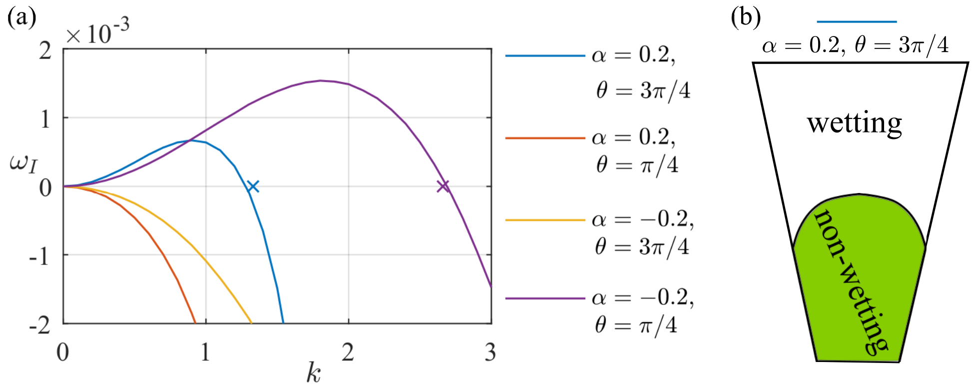

Figure 2: (a) Growth rate, ω_I as a function of wave number k in the case of equal density fluids ($R = 1$). The curves are calculated using the method in §3. The critical wavenumbers predicted by (4.3) are shown as crosses. We use $Bo = 5$, $h = 0.5$, $b_0 = 0.3$, $M = 2$, $\mathcal{A} = 1$ and $C = 1$. (b) Schematic corresponding to the blue curve.

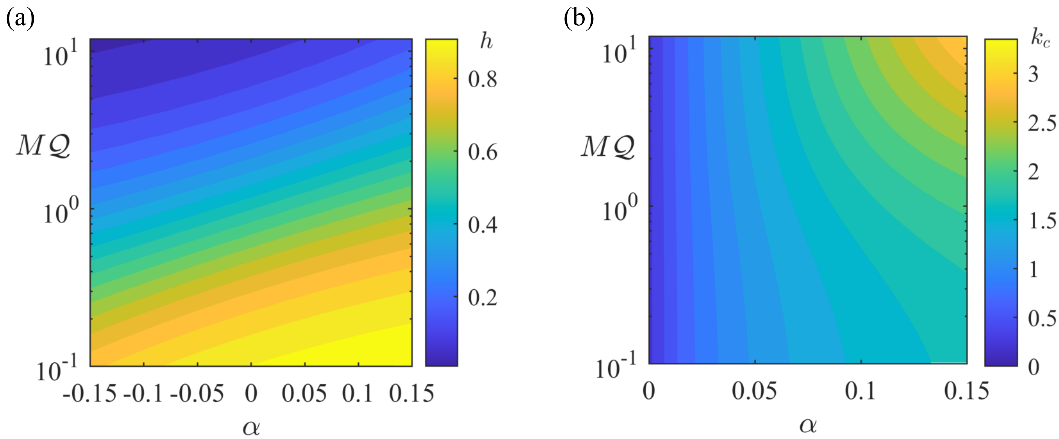

Figure 3: (a) The interface height, h, as a function of the relative flux and viscosity, and the channel angle, α for a fixed dimensionless channel area of 0.2. (b) The corresponding critical wavenumber, k_c above which the system is stable according to (4.3) for $\theta = 3\pi/4$. Note that the system is stable for all k for $\alpha \leqslant 0$.

In general, $J > 0$ is associated with instability and $J < 0$ is associated with stability. The first term, $R - 1$ represents the density difference between the fluids. It stabilizes the interface for $R < 1$ and destabilizes it for $R > 1$. The term, $-Bo^{-1}k^2$ stabilizes the interface; it arises from surface tension suppressing the curvature in the along-channel (x) direction. The final term $-2Bo^{-1}\alpha\cos\theta/b(h)^2$ is associated with surface tension acting on the curvature across the thickness of the cell. It drives or suppresses an instability depending on whether the wetting or non-wetting fluid is in the thinner part of the channel. This corresponds to the sign of α and the sign of $\cos\theta$. To interpret the instability, we consider the simpler cases of equal density in §4.1, parallel walls in §4.2 before returning to the full problem in §4.3.

4.1. *Equal density* ($R = 1$)

In the case of equal density fluids, $R = 1$, the pressure jump reduces to

$$J = -Bo^{-1}\left[k^2 + 2\alpha\cos\theta/b(h)^2\right]. \tag{4.2}$$

For small wavenumber, k, the cross-cell surface tension term controls the stability as demonstrated in figure 2a. The red and yellow curves correspond to the non-wetting fluid occupying the thicker part of the channel and the system is stable as this fluid will remain in the thicker part of the channel. The blue and purple curves represent the converse situation in which the non-wetting fluid is in the thinner part of the channel and it will move to the wider side of the channel leading to an instability (see figure 2b). For larger wavenumbers, the along-channel term stabilizes the interface. The along-channel and cross-channel curvature terms balance ($Bo^{-1}k^2 + 2Bo^{-1}\alpha\cos\theta/b(h)^2 = 0$) at a critical wavenumber,

$$k_c = \frac{\sqrt{-2\alpha\cos\theta}}{b(h)}. \tag{4.3}$$

For $k > k_c$, we anticipate that the system is stable. The critical wave numbers are shown by crosses for the two unstable setups in figure 2, demonstrating good agreement with the predictions from §3. The small discrepancy between the prediction of J (4.3) and the numerical results arises because of the physical effects, such as inertia, that are incorporated in the numerics but are negelected when using J as an approximation of the stability criterion.

In many settings, it is important to understand how the instability depends on the flux in each layer. To analyse this, we calculate the relative flux, Q of the top to the bottom layer,

$$Q = \frac{Q_2}{Q_1} = M^{-1}\frac{(b_0+\alpha)^3 - (b_0+\alpha h)^3}{(b_0+\alpha h)^3 - b_0^3}. \tag{4.4}$$

The quantity $MQ = \mu_2 Q_2/(\mu_1 Q_1)$ depends only on α, h and b_0. We consider channels of fixed dimensionless area so that

$$\int_0^1 b(y)\,\mathrm{d}y = b_0 + \alpha/2 = \text{constant}. \tag{4.5}$$

For a given channel area and relative flux, Q, we can calculate the interface height h as a function of the channel angle α (see figure 3a for the case with dimensionless area 0.2). We can also calculate the critical wavenumber, k_c by using (4.3) (see figure 3b for the case $\theta = 3\pi/4$).

4.2. *Parallel cell walls ($\alpha = 0$)*

In the case that the cell walls are parallel,

$$J = R - 1 - Bo^{-1}k^2. \tag{4.6}$$

For small k, the stability is controlled solely by the density ratio, R. In the case that $R < 1$, the system is stabilised by the density difference and there are no destabilizing effects (Gondret & Rabaud 1997). For $R > 1$, the Rayleigh-Taylor instability is stabilised for large k owing to the along cell surface tension. Neutral stability is given by

$$k_c = \sqrt{Bo(R-1)}. \tag{4.7}$$

Figure 4 shows the growth rate as a function of wavenumber (obtained in §3). For $R > 1$, the critical wavenumber prediction is indicated by crosses, showing good agreement.

4.3. *Competition between density difference and surface tension*

The cross-cell surface tension effect may be nullified or complemented by buoyancy, depending on whether the wetting or non-wetting fluid is denser. The critical value of R

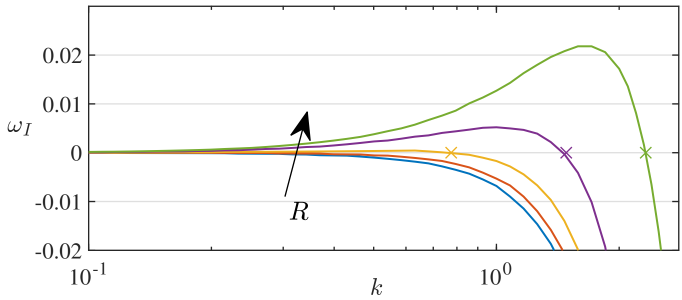

Figure 4: Growth rate, ω_I as a function of wave number, k, in the case of parallel cell walls ($\alpha = 0$) calculated using the method of §3. The density ratio is $R = 0.4, 0.8, 1.6, 3.2, 6.4$. The crosses correspond to the critical wavenumber for neutral stability for $R > 1$ given by (4.7). We use $h = 0.5$, $b_0 = 0.3$, $M = 2$, $\mathcal{A} = 1$, $C = 1$ and $Bo = 1$.

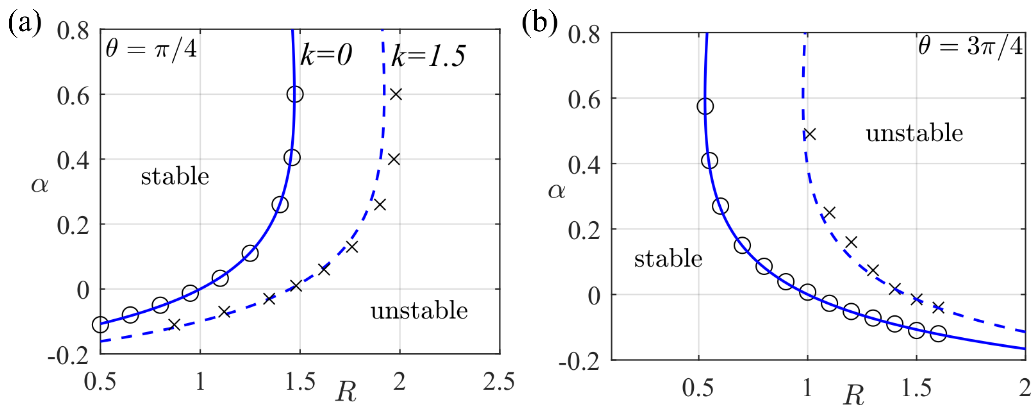

Figure 5: Neutral stability curves for (a) $\theta = \pi/4$ and (b) $\theta = 3\pi/4$. Blue lines show the predictions of (4.8) for $k = 0$ and $k = 1.5$. Circles and crosses show the results from §3 for $k = 0.2, 1.5$, respectively. We use $Bo = 5$, $h = 0.5$, $b_0 = 0.3$, $M = 2$, $\mathcal{A} = 1$ and $C = 1$.

corresponding to neutral stability is (see 4.1)

$$R_c(k) = 1 + \frac{k^2}{Bo} + \frac{2\alpha\cos\theta}{Bo(b_0 + \alpha h)^2}. \tag{4.8}$$

The system is stable for all wavenumbers when $R < R_c(0)$, which is shown as a continuous blue line in figure 5. The results from §3 for neutral stability for $k = 0.2$ are plotted as black circles showing good agreement. A comparison is also shown for $k = 1.5$ as a broken blue line.

Figure 6 shows the critical density ratio $R_c(0)$ as a function of the relative flux, and the channel inclination α in the case of a constant cell area, 0.2. The interface height, h is obtained from (4.4). When α is small, the critical density ratio becomes independent of the relative flux (and hence the interface height, h) because wetting effects become unimportant.

5. Conclusion

We have obtained the dispersion relation for the co-flow of two immiscible fluids in a Hele-Shaw cell with vertically varying gap width. The stability of the system is accurately predicted

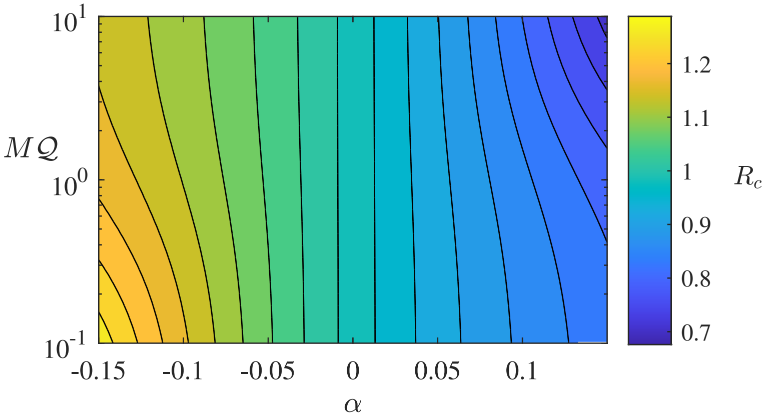

Figure 6: Critical value of R corresponding to neutral stability from (4.8) as a function of cell wall inclination, α, and relative flux QM for $k = 0$, $\theta = 3\pi/4$, $Bo = 5$. The cell area is fixed as 0.2 and the interface position is given in figure 3a.

by the sign of the quantity

$$J = R - 1 - Bo^{-1}\left[k^2 + 2\alpha\cos\theta/b(h)^2\right]. \tag{5.1}$$

The last term, associated with channel wall inclination, represents the preference of the non-wetting fluid to occupy the thicker part of the channel. The interface is stable when the fluids have equal density and the wetting fluid occupies the thinner part of the channel. A density difference may complement or oppose this effect. We have obtained critical values of the density ratio, R, below which the system is stable to all wave-numbers. Our results also provide a basis for exploring the stability of important but more complex situations such as cells with elastic walls and cells whose vertical structure varies in the horizontal direction (e.g. Pihler-Puzović *et al.* 2013).

Declaration of Interests: The authors report no conflict of interest.

Appendix A. Coefficients for Frobenius' method

In either fluid, the governing equation takes the form

$$(\bar{b}^2+a_4\bar{b}^4+a_6\bar{b}^6)v_{\bar{b}\bar{b}}+(-\bar{b}+a_4\bar{b}^3+a_6\bar{b}^5)v_{\bar{b}}+(-3+(-1-a_4)\bar{b}^2-(a_4+a_6)\bar{b}^4-a_6\bar{b}^6)v = 0. \tag{A 1}$$

The indicial polynomial is $n^2 - 2n - 3 = 0$, which has solutions, $n = 3$ and $n = -1$. We write the first power series of $v(\bar{b})$ as

$$\Phi(x) = x^3 \sum_0^\infty P_n x^n, \tag{A 2}$$

with $P_0 = 1$ and the recurrence relation

$$P_n\left[n^2 + 4n\right] + P_{n-2}\left[n(n+2)a_4 - 1\right] + P_{n-4}\left[a_6(n^2 - 2n) - a_4\right] - P_{n-6}a_6 = 0 \tag{A 3}$$

The second independent power series solution is given by

$$\Psi(x) = \Phi(x)\log x + x^{-1}\sum_0^\infty Q_n x^n, \tag{A 4}$$

where $Q_0 = 16/(4a_4 - 1)$, $Q_2 = -Q_0/4$, $Q_4 = 1$ and

$$0 = (n^2 - 4n)Q_n + Q_{n-2}\big[a_4(n-2)(n-4) - 1\big] + Q_{n-4}\big[a_6(n-4)(n-6) - a_4\big] \tag{A 5}$$

$$- Q_{n-6}a_6 + P_{n-4}(2n-4) + P_{n-6}a_4(2n-6) + P_{n-8}a_6(2n-10). \tag{A 6}$$

REFERENCES

Al-Housseiny, T. T., Tsai, P. A. & Stone, H. A. 2012 Control of interfacial instabilities using flow geometry. *Nature Physics* **8** (10), 747–750.

Benham, G. P., Bickle, M. J. & Neufeld, J. A. 2021 Upscaling multiphase viscous-to-capillary transitions in heterogeneous porous media. *Journal of Fluid Mechanics* **911**, A59.

Dias, E. O. & Miranda, J. A. 2013 Taper-induced control of viscous fingering in variable-gap Hele-Shaw flows. *Physical Review E* **87** (5), 053015.

Gondret, P. & Rabaud, M. 1997 Shear instability of two-fluid parallel flow in a Hele–Shaw cell. *Physics of Fluids* **9** (11), 3267–3274.

Grenfell-Shaw, J. C. & Woods, A. W. 2017 The instability of a moving interface in a narrow tapering channel of finite length. *Journal of Fluid Mechanics* **831**, 252–270.

Homsy, G. M. 1987 Viscous fingering in porous media. *Annual review of fluid mechanics* **19** (1), 271–311.

Huang, Z., Yang, Q., Su, M., Li, Z., Hu, X., Li, Y., Pan, Q., Ren, W., Li, F. & Song, Y. 2018 A general approach for fluid patterning and application in fabricating microdevices. *Advanced Materials* **30** (31), 1802172.

Loewenherz, D. S. & Lawrence, C. J. 1989 The effect of viscosity stratification on the stability of a free surface flow at low Reynolds number. *Physics of Fluids A: Fluid Dynamics* **1** (10), 1686–1693.

Mortimer, P. K. & Woods, A. W. 2021 Immiscible capillary flows in non-uniform channels. *Journal of Fluid Mechanics; In Press* .

Park, C-W & Homsy, G. M. 1984 Two-phase displacement in Hele Shaw cells: theory. *Journal of Fluid Mechanics* **139**, 291–308.

Pihler-Puzović, D., Périllat, R., Russell, M., Juel, A. & Heil, M. 2013 Modelling the suppression of viscous fingering in elastic-walled Hele-Shaw cells. *Journal of Fluid Mechanics* **731**, 162–183.

Rabaud, M. & Moisy, F. 2020 The Kelvin–Helmholtz instability, a useful model for wind-wave generation? *Comptes Rendus. Mécanique* **348** (6-7), 489–500.

Romero, L. A. & Yost, F. G. 1996 Flow in an open channel capillary. *Journal of Fluid Mechanics* **322**, 109–129.

Saffman, P. G. & Taylor, G. I. 1958 The penetration of a fluid into a porous medium or Hele-Shaw cell containing a more viscous liquid. *Proceedings of the Royal Society of London. Series A. Mathematical and Physical Sciences* **245** (1242), 312–329.

Sauer, C. W. 1987 Mud displacement during cementing state of the art. *Journal of Petroleum Technology* **39** (09), 1–091.

Weislogel, M. M. & Lichter, S. H. 1996 A spreading drop in an interior corner: theory and experiment. *Microgravity Science and Technology* **9** (3), 175–184.

Woods, A. W & Mingotti, N. 2016 Topographic viscous fingering: fluid–fluid displacement in a channel of non-uniform gap width. *Philosophical Transactions of the Royal Society A: Mathematical, Physical and Engineering Sciences* **374** (2078), 20150427.

Yih, Chia-Shun 1967 Instability due to viscosity stratification. *Journal of Fluid Mechanics* **27** (2), 337–352.

Zeybek, M. & Yortsos, Y. C. 1992 Parallel flow in Hele-Shaw cells. *Journal of Fluid Mechanics* **241**, 421–442.

Zhao, B., MacMinn, C. W., Primkulov, B. K., Chen, Y., Valocchi, A. J., Zhao, J., Kang, Q., Bruning, K., McClure, J. E., Miller, C. T. & others 2019 Comprehensive comparison of pore-scale models for multiphase flow in porous media. *Proceedings of the National Academy of Sciences* **116** (28), 13799–13806.